SOL ENGINEERING SERVICES

Additively Manufactured Jet-Impingement Cold Plates with Interleaved Returns

Published printed coolers, interleaved-return performance, design-for-additive-manufacturing limits, topology optimization and tests of the CF-JET geometry claims

Prepared for DEVCOM Army Research Laboratory, the Ground Vehicle Systems Center, and university and industry partners of the CF-JET effort

Classification	Unclassified. Prepared from open-source information.
Date	23 November 2026

Executive Summary

Additive manufacturing has produced working liquid coolers with manifold and impingement geometry, and the measured evidence stops well short of the CF-JET concept. The best peer-reviewed measurement found is a one-piece aluminum manifold-microchannel sink that dissipated 132 to 224 W/cm² on a 1 cm² heated area at a total resistance of 0.35 to 0.21 K/W, which is 21 to 35 mm²·K/W (derived).[1] The CF-JET design point of 1.5 kW on a 60 mm by 60 mm footprint and a target of 0.02 K/W equals 72 mm²·K/W on 36 cm², which is 36 times the area of that test (derived).[2] No peer-reviewed measurement of a metal printed jet array with interleaved returns near that footprint was retrieved, and the sections of this paper establish what the published record supports and where the CF-JET claims rest on extrapolation.

- **Published coolers.** Measured printed coolers reach 21 to 94 mm²·K/W on footprints of 1.0 to 1.44 cm² (Table 1, Figure 2).[3,4] The printed jet-impingement plates in the literature are mostly numerical, built in photopolymer or reported by companies without process data (Table 2).[5,6,7]
- **Interleaved and manifold returns.** Against a reference microchannel sink, the printed manifold design lowered resistance by 24.2 to 44.0 percent and pressure drop by 37.9 to 70.2 percent at 100 W/cm². In another printed study, a manifold cut pressure drop by about 90 percent at Reynolds numbers near 210 and raised resistance (Table 3).[8,9]
- **Design-for-AM limits.** In an Inconel 718 study, vertical 1 mm channels built to 988 µm equivalent diameter and horizontal ones to 805 µm, and 500 µm channels were partly blocked at build angles of 22.5° or less.[10] A 19.5 percent undersize raises the ideal pressure drop of a nozzle by a factor of 2.4 (derived, Table 4).
- **Topology optimization.** Published work optimizes manifold flow distribution and microchannel layouts, and a bi-level jet and microchannel heat sink built by laser powder bed fusion showed pressure drops 8.8 to 30.9 percent above the design because of printed imperfections.[11] No validated topology optimization of a jet array with interleaved returns was retrieved (Table 6).
- **Claims tested.** About 100 to 150 jets on 3600 mm² imply a pitch of 4.9 to 6.0 mm, inside the claimed 3 to 8 mm grid. Across 0.5 to 2 mm jets, the design flows of 4 to 8 L/min give jet velocities of 0.14 to 6.8 m/s, and the ideal nozzle pressure drop reaches 23.7 kPa for 0.5 mm jets, with 48.5 kPa at a discharge coefficient of 0.7 (derived, Table 8).

The implications for CF-JET are specific. Jets below about 0.56 mm in diameter exceed the 30 kPa limit at the high end of flow and the low end of jet count if the discharge coefficient is 0.7 (derived). Orifices should be built with their axes along the build direction, and as-built diameters should be measured by computed tomography before the thermal tests. The one-piece claim has support for printed metal bodies and has no published demonstration for a jet plate with return passages and a separate target plate.

1. Introduction and Scope

A jet-impingement cold plate needs a plenum that feeds many small orifices, a gap between the orifices and the target, and return passages that remove the spent coolant without sweeping it across downstream jets. Conventional manufacture builds these as stacked and brazed or bonded parts. Additive manufacturing offers a single build in which the manifold, the orifices and the return passages share one body, and the question for a program is how much of that promise has been shown with hardware and where the process limits lie.

This paper answers four questions: which additively manufactured jet-impingement and manifold-

microchannel coolers have been published and what performance they reported; how interleaved-return designs compare with conventional arrays in heat transfer and pressure drop; which design-for-additive-manufacturing limits apply to nozzle diameter, wall thickness, surface roughness, powder and support removal and dimensional tolerance; and how topology optimization has been applied to flow-distribution manifolds. It then tests three claims from the CF-JET concept: about 100 to 150 jets of 0.5 to 2 mm diameter on a 3 to 8 mm grid, an impingement gap of 1 to 3 mm, and one-piece construction with no brazed joints.[12]

The reference design point is 1.5 kW on a 60 mm by 60 mm footprint with 50/50 water-glycol at 65 °C inlet, 4 to 8 L/min and a pressure drop of 30 kPa or less. These are SOL proposal assumptions, and the case-to-coolant target of 0.02 K/W corresponds to 72 mm²·K/W on the footprint (derived).[13] Area-normalized resistance lets the paper compare coolers of different size, and each conversion multiplies the reported K/W by the area stated in the source. The coolant properties used in the jet calculations are assumptions stated where they appear, because the retrieved sources do not give them for this fluid. Figure 1 shows the operational concept and the scope of the paper.

Figure 1. Operational concept of the CF-JET cold plate and scope of the paper

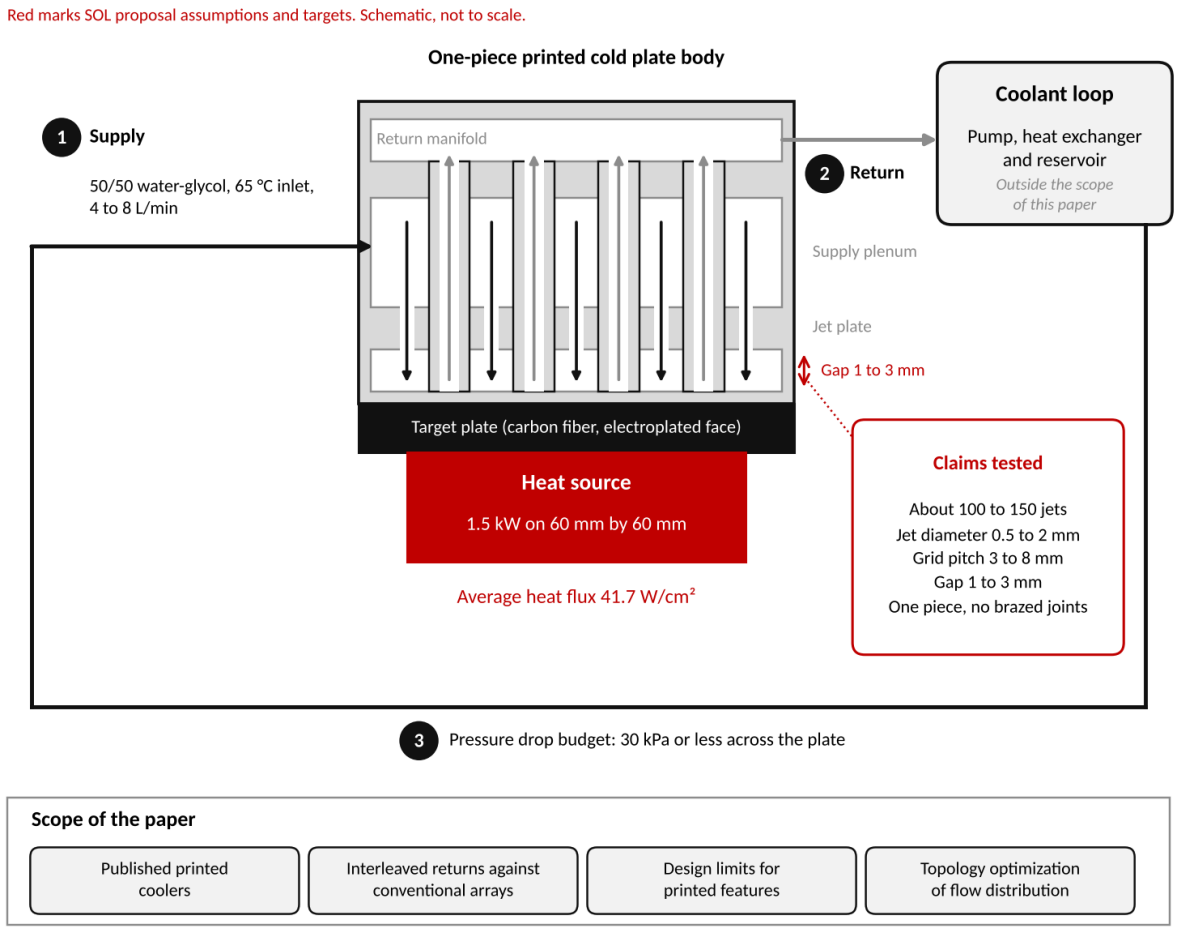

Operating conditions and geometry are SOL proposal assumptions.[14] *The diagram is schematic and not to scale.*

2. Published Additively Manufactured Impingement and Manifold

Coolers

2.1 Measured printed coolers reach 21 to 94 mm²·K/W on footprints of 1.0 to 1.44 cm²

Kong et al. printed a manifold-microchannel heat sink as one aluminum part by laser powder bed fusion on an EOS M290, using AlSi10Mg powder, and tested it in a closed water loop.[15] The part measures 30 mm by 15 mm by 9 mm with a heated area of 10 mm by 10 mm. The manifold has six inlet and seven outlet branches that taper from 0.45 mm at the inlet to 1.25 mm at the outlet, and 21 microchannels of 0.2 mm width and 2.0 mm height are cut beneath it. The fin and manifold walls are 0.3 mm thick, which the authors state as the minimum feature size of their process.[16] Flow of 100 to 400 g/min produced pressure drops of 0.15 to 1.7 kPa and total resistances of 0.35 to 0.21 K/W, and the sink dissipated 132 to 224 W/cm² at a bottom surface temperature of 100 °C. The abstract states up to 240 W/cm², and the results section gives the lower maximum, so the paper uses the results values.[17]

Collins et al. at Purdue built straight and manifold microchannel heat sinks in AlSi10Mg by direct metal laser sintering with 500 µm hydraulic diameters. The measured resistances were 0.29 to 0.50 K/W for the straight design and 0.45 to 0.65 K/W for the manifold design on 1.44 cm², and the printed material had a surface roughness (Ra) of about 20 µm and a conductivity of 110 W/m·K.[18] Table 1 lists these studies with the printed impingement plates found, and Figure 2 plots the area-normalized resistances against the CF-JET target.

Table 1. Published additively manufactured and printed impingement and manifold coolers

Study	Process and material	Geometry and test	Reported result	Evidence
Kong et al., 2023[19]	LPBF, AlSi10Mg, one piece, heat treated 2 h at 300 °C	Six inlet and seven outlet manifold branches; 21 channels of 0.2 mm by 2.0 mm; 0.3 mm walls; 10 mm by 10 mm heated area; water at 100 to 400 g/min	0.35 to 0.21 K/W; 0.15 to 1.7 kPa; 132 to 224 W/cm² at 100 °C bottom surface	Peer-reviewed; measured
Collins et al., 2019[20]	DMLS, AlSi10Mg	Straight and manifold microchannels; 500 µm hydraulic diameter; 1.44 cm²	Straight 0.29 to 0.50 K/W; manifold 0.45 to 0.65 K/W; Ra about 20 µm; 110 W/m·K	Peer-reviewed; measured
Hoang et al., 2022[21]	Printed AlSi10Mg and copper alloy plates	Impingement pin-fin plate; 6.45 cm²	Aluminum 0.064 to 0.067 K/W at 2 L/min and 21.1 to 28.1 kPa; copper alloy 0.048 K/W at 1 L/min and 8.14 kPa	Peer-reviewed; numerical
Sun et al., 2026[22]	LPBF; parts scanned by computed tomography	Jet impingement manifold with topology-optimized microchannels; three inlet-outlet layouts; 83.3 to 200 W/cm²	Best simulated case 51.3 °C average and 54.0 °C peak at 200 W/cm² and 31.0 kPa; imperfections raised pressure drop by 8.8% to 30.9%	Peer-reviewed; measured and numerical
Hobby et al., 2021[23]	Photopolymer print	Interspersed extraction ports; water	Pressure drop matched simulation after manifold losses were added; heat transfer matched reasonably with differing trends	Peer-reviewed; experiment and simulation
NREL traction inverter, 2020[24]	Plastic jet prototypes	Three cooling configurations at full inverter power	Higher thermal performance with jets than with the channel baseline	Peer-reviewed preprint; measured

Resistance values are as reported. The area-normalized values in Figure 2 multiply the reported K/W by the stated area. The Kong et al.

resistance is the paper's total resistance, and its experiment showed a 37.4% difference between total and effective heat, so the area-normalized values carry that uncertainty.

Figure 2. Area-normalized resistance of printed coolers against the CF-JET target

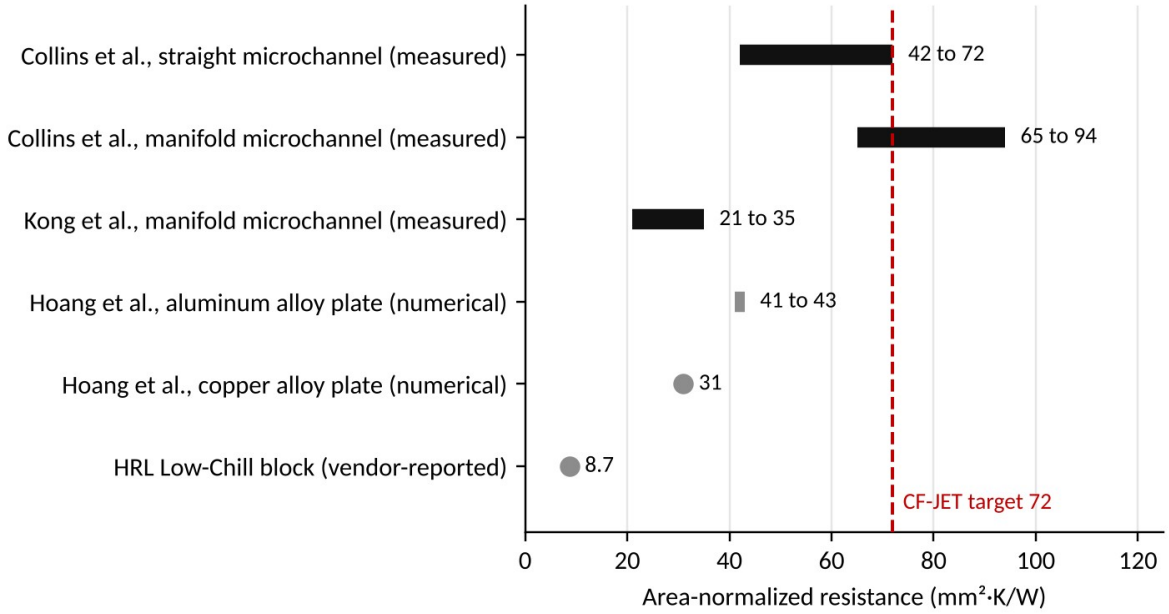

Black bars are peer-reviewed measurements. Grey marks are numerical results or a vendor-reported value. The Kong et al. and HRL values are derived in this paper from the reported K/W and the stated areas of 1 cm² and 10.6 cm². The red dashed line marks the 72 mm²·K/W target.

The measured printed values at 21 to 94 mm²·K/W straddle the CF-JET target of 72 mm²·K/W, and the lowest one is 3.4 times lower than the target (derived). The comparison has two limits. The footprints are 1.0 and 1.44 cm², and the CF-JET plate is 25 to 36 times larger (derived), so the spreading and flow-distribution burden is greater. The Kong et al. heat flux of 132 to 224 W/cm² is 3.2 to 5.4 times the 41.7 W/cm² average of the CF-JET design point (derived), so that sink operates in a different regime.

2.2 Printed jet plates appear mostly in simulation or in polymer

Hoang et al. report the design and analysis of printed impingement pin-fin plates in aluminum and copper alloys, and their resistances are numerical.[25] Hobby et al. printed a water device with interspersed extraction ports in photopolymer and compared it with simulation, finding that the pressure drop agreed only after manifold losses were added.[26] Wei describes a polymer multi-jet cooler in which the outlet plenum accounted for 57 percent of the pressure drop at 1,000 mL/min.[27] The NREL work on a traction drive inverter tested a baseline channel exchanger, jets on a plain surface and jets on a microfinned surface at full inverter power, and the plastic jet prototypes performed better than the channel baseline.[28] A separate NREL project on a light-weight cold plate reported that a glass-fiber reinforced nylon construction saved about half of the assembly mass.[29]

Sun et al. built a bi-level heat sink by laser powder bed fusion that pairs jet impingement manifolds with topology-optimized microchannels, scanned the parts by computed tomography and tested three inlet-outlet layouts at 83.3 to 200 W/cm². Their best simulated layout, with four inlets and five outlets, gave an average temperature of 51.3 °C and a peak of 54.0 °C at 200 W/cm² with a pressure drop of 31.0 kPa.[30] The pressure drop of 31.0 kPa is the same size as the CF-JET limit of 30 kPa at a heat flux 4.8 times the CF-JET

average (derived), and the study quantifies how printed imperfections change a simulated design, which Table 6 lists.

2.3 Georgia Tech, Purdue, Stanford and NREL contributions differ in kind

Purdue contributed the measured printed microchannel and manifold data, a topology optimization method for microchannel sinks and a dissertation on the effect of internal channel roughness in printed microchannel sinks.[313233] Georgia Tech appears twice in the record: Pahinkar et al., with Army Research Laboratory co-authors, studied liquid-cooled jet-array heat sinks in a numerical study, and Johnstone, Saldana and Saleeby measured the dimensional accuracy of thin walls in laser powder bed fusion.[3435] NREL contributed the inverter tests and the light-weight plate.[3637] No Stanford publication on single-phase additively manufactured impingement or manifold coolers was retrieved, and the paper makes no statement about Stanford work beyond that gap.

2.4 Company-reported products disclose results and omit process data

JetCool describes microjets of less than a millimeter in diameter that impinge directly on the cooled surface, and a press release states that its SmartPlate reduced the thermal resistance of an NVIDIA H100 GPU from 0.122 °C/W to 0.021 °C/W.[3839] The company web page states a thermal resistance 20 to 40 percent lower than state-of-the-art microchannel cold plates.[40] In an ARPA-E COOLERCHIPS kickoff presentation, JetCool listed a case-to-fluid resistance target of 0.009 K/W, a cooling power below 3 percent of IT power, and federal funding of $1.26 million over 24 months.[41] The sources retrieved do not state how the SmartPlate jet plates are manufactured.

HRL Laboratories describes Low-Chill, a block that mates a 3D-printed manifold with interwoven inflow and outflow channels to a conventional skived fin plate. The white paper reports a resistance of 8.2 °C/kW on a 1 kW, 10.6 cm² test vehicle, pumping power below 5 W per kW, and a pressure drop more than 10 times lower than a commercial block.[42] The manifold can be printed in copper alloys, stainless steels or high-temperature polymers, and prototypes were printed in plastic. The white paper gives no flow rates and no minimum feature sizes, and it is a document written to attract licensees. CoolIT Systems states that its split-flow cold plates typically show upwards of 60 percent lower thermal resistance than standard cold plate designs, and the tech brief does not state a manufacturing process.[43] Table 2 lists the company claims.

Table 2. Company-reported impingement and manifold cooling products and targets

Organization and product	Reported claim	Basis	Process disclosure
JetCool SmartPlate[44]	H100 GPU resistance from 0.122 °C/W to 0.021 °C/W; 2% of cooled power for pumping	Press release, vendor-reported	Not stated in the sources read
JetCool microconvective cooling[4546]	20% to 40% lower resistance than microchannel cold plates; jets under 1 mm	Vendor web page and trade article	Not stated in the sources read
JetCool Sub-One system[47]	Target of 0.009 K/W case to fluid; funding of $1.26 million over 24 months	Government program presentation; a target and not a result	Not applicable
HRL Low-Chill[48]	8.2 °C/kW on a 10.6 cm² test vehicle (8.7 mm²·K/W, derived); pressure drop more than 10 times lower than a commercial block	Laboratory white paper, vendor-reported	Printed manifold in copper alloy, steel or polymer; mates to a skived fin plate

Organization and product	Reported claim	Basis	Process disclosure
CoolIT split-flow[49]	Typically upwards of 60% lower resistance than standard cold plates	Vendor tech brief	Not stated in the sources read

Company claims are used for product facts and are not independent evidence. The JetCool Sub-One value is a program target. The HRL area-normalized value multiplies 0.0082 K/W by 10.6 cm².

3. Interleaved Returns Compared with Conventional Arrays

3.1 Printed manifolds cut pressure drop by 38 to 90 percent in measured studies and trade resistance in one

The clearest comparison in the printed literature is between manifold designs, which alternate inlet and outlet branches over short channels, and conventional channels that carry the flow along their full length. Kong et al. compared their manifold-microchannel sink with a conventional microchannel sink taken from the literature at 100 W/cm². The printed manifold gave a resistance 24.2 to 44.0 percent lower, a pressure drop 37.9 to 70.2 percent lower and a coefficient of performance 1.7 to 3.6 times higher.[50] The baseline sink came from the literature and was built by a different process, so surface roughness and material differ between the two.

Collins et al. built both designs in the same process and found a different balance. The manifold design reduced pressure drop by about 90 percent at a Reynolds number near 210 and by about 40 percent near 1,175, and its resistance of 0.45 to 0.65 K/W was higher than the 0.29 to 0.50 K/W of the straight channels.[51] Table 3 shows that the two printed studies agree on the pressure drop benefit and disagree on resistance. The difference may come from the channel dimensions and the flow ranges, and the sources do not separate the causes.

Table 3. Comparisons of manifold and interleaved designs with conventional baselines

Comparison	Heat transfer	Pressure drop	Basis and caveat
Printed manifold microchannel against a literature microchannel sink at 100 W/cm²[52]	Resistance 24.2% to 44.0% lower	37.9% to 70.2% lower; coefficient of performance 1.7 to 3.6 times	Baseline from another source; measured
Printed manifold against printed straight channels, same process[53]	Resistance higher: 0.45 to 0.65 K/W against 0.29 to 0.50 K/W	About 90% lower at Re near 210; about 40% lower near 1,175	Same process and area; measured
Manifold with three channels on a pin-fin plate against a commercial plate[54]	0.061 to 0.054 °C/W; seven channels cut resistance by 16.4%	Lower by 0.77 kPa with three channels; below 0.6 kPa with seven	Largely numerical
HRL printed manifold against a commercial block[55]	8.2 °C/kW; 40% higher dissipation at similar conditions	More than 10 times lower	Vendor-reported; no flow rates
Spent-air exits between jets against single-edge exit, 3×3 array[56]	Coefficient raised; optimum nozzle spacing moved	Not stated in the source read	Air; measured

Percentages are as reported by each source. Baselines differ in manufacturing process, fluid and size, so the rows compare a design family against its own baseline and do not rank the designs.

3.2 Distributed returns for jets are validated in air, in polymer and at small footprints

Interleaved return ports for jet arrays have simulation, correlation and small-scale experimental support. Huber and Viskanta found that spent-air exits between the jets of a confined 3×3 array raised the heat transfer coefficient and changed the optimum nozzle spacing.[57] Rattner simulated more than 1,000 cases of arrays with interspersed extraction ports and fitted correlations for Nusselt number and pressure-drop loss coefficients, and Hobby extended the work with experiments on nine geometries across Prandtl numbers of 0.7 to 21.[5859] Brunschwiler et al. described a distributed return that scales to 40,000 cells on 4 cm² at jet sizes of 31 to 126 µm in silicon.[60] The largest footprint in these sources is 6.5 cm², and the CF-JET plate is 5.5 times larger (derived).

The printed examples add one finding that the planar studies lack. Hobby et al. needed to model the manifold losses to match their measured pressure drop, and Wei reports an outlet plenum at 57 percent of the total.[6162] In a printed body the supply and return plenums are part of the design space, so their losses scale with the same geometry freedom that the process offers. Figure 3 contrasts the flow path of a conventional array with that of an interleaved layout.

Figure 3. Flow paths in a conventional jet array and in an interleaved supply and return layout

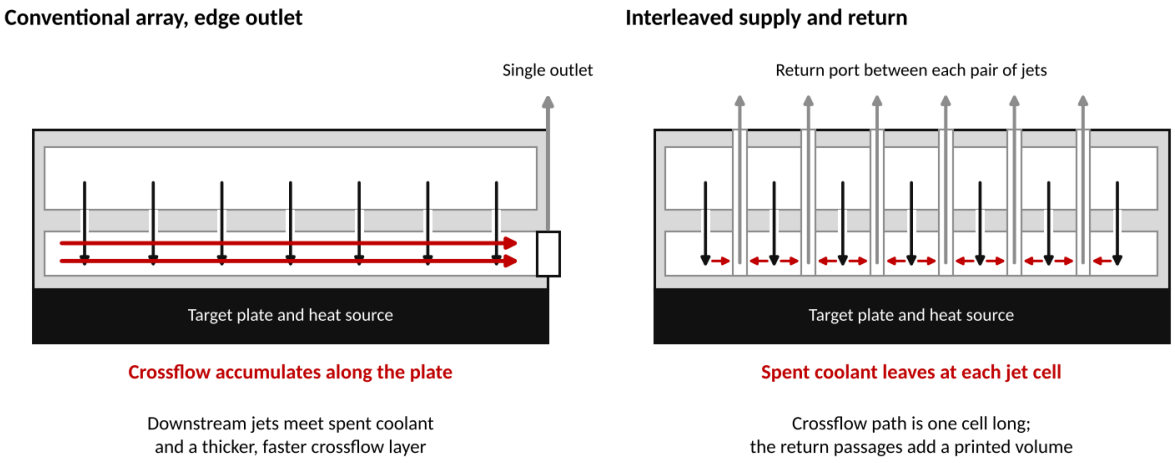

Schematic cross-sections, not to scale. The arrows indicate the intended flow paths of each concept and are not simulation results.

3.3 The pressure drop is divided among the manifold, the nozzles and the channels

Kong et al. report a computed pressure drop partition for their manifold-microchannel sink: 47.1 percent in the contraction at the manifold inlet, 36.6 percent in the microchannels, 13.3 percent in the inlet plenum and 3.1 percent in the outlet expansion.[63] The microchannels are 37 percent of the total, so 63 percent comes from the manifold structure. The partition belongs to a channel design and does not transfer to jets, and it shows that in a printed manifold the delivery path can use more of the pressure budget than the heat transfer surface. For a jet plate the nozzle plays the role of the contraction, and Table 8 quantifies the nozzle pressure drop at the CF-JET flows. Figure 4 sets the measured partition beside the nozzle share of the CF-JET limit.

Figure 4. Measured pressure drop partition of a printed manifold-microchannel sink and nozzle share of the CF-JET limit

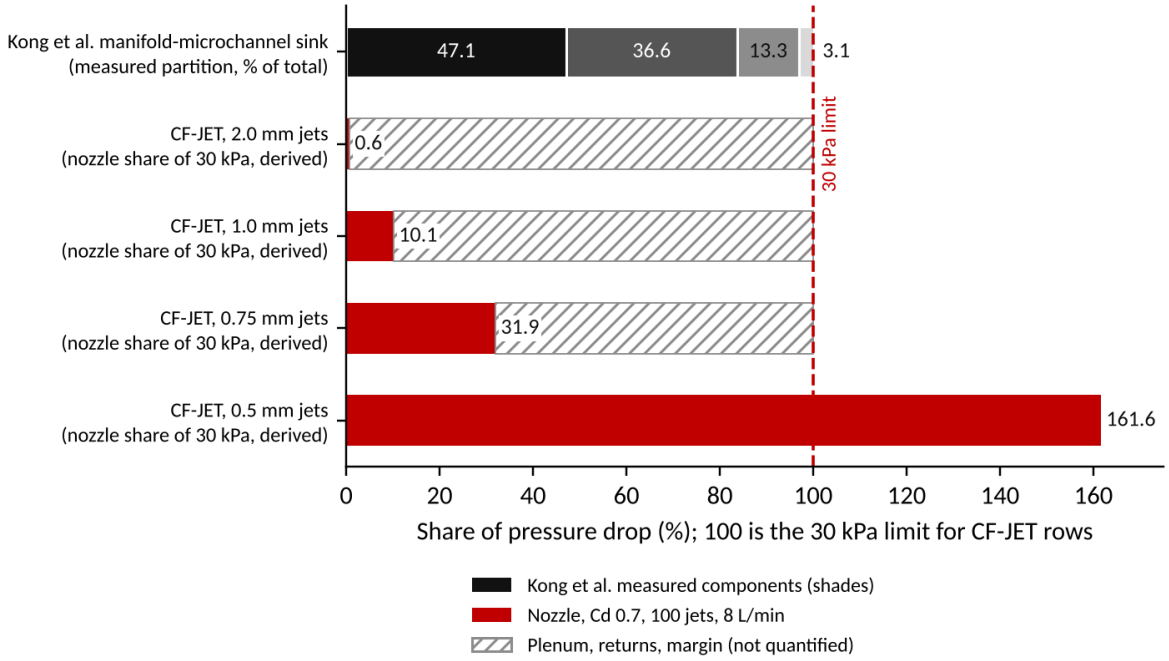

The Kong et al. partition is a computed result for a 1 cm² sink.[64] The CF-JET nozzle shares are derived at 100 jets, 8 L/min, a discharge coefficient of 0.7 and an assumed density of 1,030 kg/m³. Shares above 100 percent exceed the limit.

At 100 jets and 8 L/min the nozzle takes 31.9 percent of the 30 kPa limit at 0.75 mm and 161.6 percent at 0.5 mm (derived). At 1 mm and above it takes 10.1 percent or less, so the plenum and return losses determine most of the budget, and the sources retrieved do not quantify those losses for a jet plate.

3.4 The reported comparisons use different baselines

The comparisons in Table 3 differ in baseline, fluid and size. Two use the same process for both designs, one uses a baseline from another publication, one is numerical, and one is vendor-reported. A program that cites these comparisons for a jet plate needs its own baseline, built in the same process and tested in the same loop. The sources reviewed give no printed jet array with and without interleaved returns tested side by side, which leaves the benefit of the return ports in a printed body as an evidence gap.

4. Design-for-Additive-Manufacturing Limits

4.1 Orifice diameter depends on build orientation as well as on the nominal value

Kasperovich et al. developed a laser powder bed fusion strategy for small internal channels in Inconel 718 and measured how build inclination changes the result.[65] Channels with a target diameter of 1,000 µm built vertically reached an equivalent diameter of 988 ± 10 µm and a roundness of 0.96. Built horizontally, the same channels reached 805 ± 26 µm and a roundness of 0.37, with melt beads of 150 to 200 µm on the downskin surface. At 45° the equivalent diameter was 952 ± 14 µm and at 22.5° it was 820 ± 22 µm. Channels with a target diameter of 500 µm were partly blocked at inclinations of 22.5° or less.[66]

A droplet cross-section that scales with the build angle, combined with optimized contour parameters, raised the roundness from about 0.4 to between 0.8 and 0.9 and removed most fusion beads at 22.5°.[67]

The study used Inconel 718 channels in test cylinders. A jet plate in AlSi10Mg has different melt behavior and a different geometry, so the results indicate the size of the effect and do not give design values for CF-JET. Two process limits from other studies bound the wall features of the jet plate. Wu, Narra and Rollett reached a minimum wall thickness of about 100 µm and a maximum inclination of 60° in Ti-6Al-4V, Inconel 718 and AlSi10Mg with optimized part design and processing conditions, and Kong et al. used 0.3 mm walls as the minimum feature of their process.[6869]

4.2 A diameter undersize of 19.5 percent raises the ideal nozzle pressure drop by a factor of 2.4

At a fixed flow rate, the velocity through an orifice scales with the inverse square of its diameter and the ideal pressure drop with the inverse fourth power.[70] Table 4 applies the measured equivalent diameters of the 1 mm channels to that scaling. A vertical build raises the pressure drop by 5 percent. A 45° build raises it by 22 percent, and the 22.5° and horizontal builds raise it by factors of 2.2 and 2.4. The droplet cross-section at 22.5° returns the factor to 1.0. The values apply to channels in Inconel 718 and show that orientation and cross-section compensation move the nozzle pressure drop by more than the likely design margin.

Table 4. Sensitivity of ideal nozzle pressure drop to as-built diameter (derived from measured channels)

Build condition	Equivalent diameter, share of target	Flow area change	Velocity factor	Pressure drop factor
Round, vertical (90°)	98.8%	−2.4%	1.02	1.05
Round, 45°	95.2%	−9.4%	1.10	1.22
Round, 22.5°	82.0%	−32.8%	1.49	2.21
Round, horizontal (0°)	80.5%	−35.2%	1.54	2.38
Droplet, horizontal (0°)	91.0%	−17.2%	1.21	1.46
Droplet, 22.5°	99.9%	−0.2%	1.00	1.00

Equivalent diameters are the means measured by Kasperovich et al. for channels of 1,000 µm target diameter in Inconel 718. The factors are derived at constant flow and ignore changes in the discharge coefficient and in the entrance condition, so they give the geometric part of the effect.[71]

4.3 Wall thickness limits are set by dross and recoater contact

Johnstone, Saldana and Saleeby printed thin 316L walls of 0.38, 0.50 and 1.00 mm thickness with slits of 1 mm by 2 mm and measured them by computed tomography. They attributed dimensional error to dross on overhanging horizontal edges and to recoater blade contact on vertical edges, and both defects were worse in thinner walls and on longer slit sides.[72] Higher laser power reduced the deflection of vertical edges and increased the dross on horizontal edges. The text reports no absolute deviations from the nominal slit size, and the only stated magnitude is a slant below 30 µm that did not depend on wall thickness.[73] The jet plate between the plenum and the impingement gap is a thin, perforated wall with long horizontal faces, and these results indicate that its underside and its orifice edges are the locations where dross collects. Ozguc, Pan and Weibel set a minimum solid fin thickness of 150 µm for DMLS in AlSi10Mg in their optimization, which is a further process-based limit on the fine features of the target side.[74]

4.4 Surface roughness is a few percent of a 0.5 mm jet on most faces and larger on downskin faces

Kong et al. measured a surface roughness (Sa) of 9.3 µm on microchannel walls and 16.2 µm on manifold walls, which they attribute to the manifold having been built above the microchannels in an unstable position.[75] Their simulation with a roughness height of 12.7 µm changed the pressure drop by about 3.9 percent. Collins et al. measured an Ra of about 20 µm on printed AlSi10Mg.[76] Kasperovich et al. found Sa of 6.8 to 7.2 µm on upskin and inskin faces and 47.5 µm on downskin faces with optimized contour parameters, and 80.5 µm on downskin faces at a lower energy input.[77] Against a 0.5 mm jet, 9.3 to 16.2 µm is 1.9 to 3.2 percent of the diameter and 47.5 µm is 9.5 percent (derived).

The effect of printed roughness on jets has been studied for holes in gas turbine cooling and for channels. In printed film cooling holes, roughness inside the hole raised convective cooling within the hole and increased jet mixing at the exit, and dross on the leeward side of the hole inlet produced the largest deviations from the design intent.[78] Studies of printed channels report roughness effects on friction factor and heat transfer, and the sources retrieved do not give a discharge coefficient for a printed 0.5 to 2 mm orifice in a liquid jet plate.[798081] Material properties change with the build and its heat treatment as well. Annealing raised the conductivity of printed AlSi10Mg by 18 to 41 percent in one study, and Kong et al. heat treated their sink for 2 hours at 300 °C to close pores and reduce leakage.[8283]

4.5 Powder removal limits the use of branching internal passages

Hunter et al. fabricated test devices with internal channels in Ti-6Al-4V and tested removal methods. Hand-held ultrasonic polishing cleared straight blind channels down to 1 mm in under 10 seconds, ultrasonic bathing and vacuum boiling removed most powder from complex devices, and ultrasonic polishing was largely unsuccessful on U-bend channels.[84] Removal was easier with larger diameters and fewer bends, powder in electron beam melted parts was partly sintered and hard to remove, and computed tomography was the most useful inspection method.[85] Kong et al. used support pillars at the plenums and an arch-shaped top cover to avoid overhang, and their paper does not describe powder removal.[86]

An interleaved supply and return manifold forms a branching internal volume with a thin gap under the jet plate. These results indicate that such a volume needs drain and access ports, a minimum of bends and a computed tomography inspection of the first articles, and the sources retrieved contain no powder removal study for a gap of 1 to 3 mm over a footprint of 60 mm by 60 mm.

4.6 Polymer processes impose larger minimum features than metal processes

A fabricator of polymer powder-bed parts states a guaranteed minimum wall thickness of 1 mm for unfinished parts, 1.5 mm for parts that will be polished or shot-peened, and a recommended minimum hole diameter of 3 mm because powder fuses into small holes and channels.[87] The statement is vendor guidance for selective laser sintering and multi-jet fusion, and it does not apply to photopolymer resin processes, in which Hobby et al. printed a water device with interspersed extraction ports.[88] HRL printed manifold prototypes in plastic for a 1U server.[89] The jets of 0.5 to 2 mm in the CF-JET concept lie below the vendor recommendation for polymer powder-bed holes and above the sizes that resin printing has produced in the sources retrieved, so the process choice matters for the polymer option.

Table 5. Design-for-additive-manufacturing limits reported in the sources reviewed

Feature	Reported limit or observation	Process and material	Relevance to the jet plate
Minimum wall	About 100 µm with optimized design and parameters; maximum inclination 60°[90]	LPBF; Ti-6Al-4V, Inconel 718, AlSi10Mg	Sets the thinnest jet plate and fin features

Feature	Reported limit or observation	Process and material	Relevance to the jet plate
Wall used in a cooler	0.3 mm, stated as the minimum feature[91]	LPBF; AlSi10Mg	Practical wall for a one-piece manifold
Vertical 1 mm channel	Equivalent diameter 988 ± 10 µm; roundness 0.96[92]	LPBF; Inconel 718	Orifices with axes along the build direction
Horizontal 1 mm channel	Equivalent diameter 805 ± 26 µm; roundness 0.37; beads of 150 to 200 µm[93]	LPBF; Inconel 718	Orifices in a plate built on its edge
500 µm channel	Partly blocked at 22.5° or less[94]	LPBF; Inconel 718	Smallest jet in the concept
Surface roughness	Sa 9.3 to 16.2 µm; Ra about 20 µm; downskin Sa 47.5 µm[959697]	LPBF; AlSi10Mg and Inconel 718	Jet and target surfaces
Thin-wall accuracy	Dross on horizontal edges; recoater contact on vertical edges; no absolute deviation reported[98]	LPBF; 316L	Underside of the jet plate
Powder removal	Ultrasonic polishing cleared straight channels to 1 mm; U-bends largely unsuccessful[99]	L-PBF and EBSM; Ti-6Al-4V	Branching supply and return passages
Pore sealing	Heat treatment for 2 h at 300 °C to close pores and reduce leakage[100]	LPBF; AlSi10Mg	Leak-tight one-piece body
Polymer powder-bed holes	Recommended minimum diameter 3 mm; wall 1 mm[101]	SLS and multi-jet fusion; vendor guidance	Limits the polymer option to larger jets
Design rules	Clauses on feature constraints, overhang and holes and channels; numerical limits not retrieved[102]	ISO/ASTM 52911-1	Source for tolerance and hole limits

The values are as reported by each source and apply to the stated process and material. The Inconel 718 channel results are test geometries and not orifices.

4.7 Dimensional tolerance data for orifices and gaps were not found

The ISO/ASTM standard for design of laser powder bed fusion of metals includes clauses on feature constraints, overhang, powder spreading and holes and channels, and the numerical limits were not available in the preview read for this paper.[103] Kong et al. report no as-built dimensions for their sink.[104] Sun et al. found channel shrinkage in their computed tomography scans and tied it to pressure drops 8.8 to 30.9 percent above the design.[105] No source retrieved gives the tolerance of a 1 to 3 mm gap over a 60 mm span or the diameter tolerance of 0.5 to 2 mm orifices in AlSi10Mg, and both quantities enter the CF-JET jet-to-target spacing and nozzle pressure drop.

5. Topology Optimization of Flow Distribution

5.1 Density-based optimization produces manifold microchannel fin layouts that are not yet validated by experiment

Zhou, Nomura and Dede applied a density-based topology optimization to the fins and channels of a manifold microchannel heat sink in a conjugate heat transfer model of laminar flow and conduction. The objective was a weighted sum of flow resistance and average base plate temperature, with weight ratios

of 0.33, 2 and 100 producing three designs, and no volume constraint.[106] The test case used 50/50 water and ethylene glycol at 0.25 L/min and 338.15 K, a base heat flux of 100 W/cm² and a copper heat sink of 36 mm by 36 mm with 160 unit cells. The authors state that the designs reach a lower base temperature at a given pressure drop than straight fins, that mesh independence is not fully studied and that experimental validation is future work.[107] The text reports no thermal resistance and no pressure drop values, which appear only in a figure.

5.2 Homogenization methods connect the optimizer to the process limit

Ozguc, Pan and Weibel represent intermediate densities as porous pin-fin microstructures with a fixed fin thickness of 150 µm, which is a limit of DMLS in AlSi10Mg, and the optimizer varies the gap between fins.[108] The test case was a 15 mm square base with a 1.5 mm hotspot and a 48/52 water and ethylene glycol coolant. The optimized topologies route coolant from open manifold-like channels toward dense pin fin arrays near the hotspot and reach lower thermal resistance at a given pressure drop than a straight microchannel sink optimized with the same objective.[109] The optimized designs contain pin gaps as small as 26.5 µm, and typical LPBF powder has a size of 15 to 45 µm, so the smallest gaps are about the size of one powder particle (derived comparison).[110][111] The study assumed smooth walls and noted that roughness of printed metal may affect small pins.

5.3 Three-dimensional models change the manifold geometry that two-dimensional models produce

Gupta, Arnaud and Hooman optimized an inlet manifold of a heat exchanger for flow distribution. Two-dimensional optimization under laminar and turbulent inlet conditions produced starkly different geometries, three-dimensional optimization of the laminar cases produced different geometry again because of the out-of-plane walls, and tests of stereolithography prints supported the conclusion that the three-dimensional model gives more accurate flow modeling and likely better flow distribution.[112] The abstract reports no maldistribution values. The regime dependence matters for a jet plate with a manifold that serves 100 to 150 orifices at flows from laminar to transitional, because a manifold optimized for one regime is not optimal in the other.

5.4 Manufacturing-aware optimization feeds back imperfections from computed tomography

Sun et al. designed a bi-level heat sink with a manufacturing-aware framework that joins macro-scale jet impingement manifolds to micro-scale topology-optimized channels, and they built it by laser powder bed fusion.[113] The computed tomography scans showed channel shrinkage and surface roughness that raised the pressure drop by 8.8 to 30.9 percent and accounted for experiment-to-simulation temperature differences of 7.2 to 16.8 percent. The layout with two inlets and one outlet had the smallest deviations, which the authors tie to its closer geometric fidelity in the scans.[114] This is the closest study to the CF-JET plate in the sources reviewed, because it combines jet manifolds, optimized internal geometry, laser powder bed fusion and measured deviations. Its jets, materials and manifold specifications were not available in the page read, and the study does not include interleaved return ports in the sense of the CF-JET concept. Table 6 lists the optimization studies.

Table 6. Topology optimization studies for manifold and flow-distribution geometry

Study	Design domain and objective	Fabrication and validation	Reported result
Zhou, Nomura and Dede[115]	Manifold microchannel unit cell 4.5 mm by 1.8 mm; weighted flow resistance and base temperature; no volume constraint	One additively fabricated example shown; experiments listed as future work	Lower base temperature at a given pressure drop than straight fins; values in a figure
Ozguc, Pan and Weibel[116]	Microchannel sink with hotspot; porous pin-fin microstructures of 150 µm fin thickness; weighted pressure drop and pseudo resistance	DMLS limits used as inputs; smooth-wall assumption; no fabrication in the text read	Pareto front better than straight channels; pin gaps down to 26.5 µm
Gupta, Arnaud and Hooman[117]	Heat-exchanger inlet manifold; flow distribution; 2D laminar and turbulent, 3D laminar	Stereolithography prints tested	2D results differ by regime; 3D models more accurate and likely give better distribution
Sun et al.[118]	Jet impingement manifolds with topology-optimized microchannels; three inlet-outlet layouts	LPBF; computed tomography; heat flux 83.3 to 200 W/cm²	Imperfections raised pressure drop by 8.8% to 30.9% and caused 7.2% to 16.8% temperature differences

Results are as reported in the abstracts and text read. Numerical values that appear only in figures are not reproduced.

No study retrieved applies topology optimization to the full CF-JET problem, a jet array on a 36 cm² footprint with interleaved returns, nozzle sizing and a layered target. The published work optimizes parts of it: the fins and channels under the jets, the manifold flow distribution and the combination of a jet manifold with optimized channels. Each study treats printed imperfections as a deviation measured after the build, and Sun et al. is the study that quantifies it.

6. Tests of the CF-JET Geometry Claims

6.1 The jet count implies a pitch of 4.9 to 6.0 mm, and the diameters extend past the correlation ranges

A uniform square grid of 100 to 150 jets over the 3600 mm² footprint has a pitch of 6.0 to 4.9 mm (derived), which is inside the claimed grid of 3 to 8 mm.[119] The full pitch range of 3 to 8 mm would give 56 to 400 jets, so the jet count in the claim uses the middle of the range. Table 7 compares the derived dimensionless spacings with the ranges of the correlations that address interspersed extraction ports.

Table 7. CF-JET jet geometry against the ranges of published correlations (derived)

Quantity	CF-JET range (derived)	Published range	Assessment
Pitch for 100 to 150 jets on 3600 mm²	4.9 to 6.0 mm	Claimed grid 3 to 8 mm	Inside the claimed grid
Pitch to diameter, S/D	2.45 to 12.0	Hobby: 2.7 to 9.1[120]; Rattner: 1.8 to 7.1[121]	Beyond the Hobby range for jets under 0.54 to 0.66 mm
Gap to diameter, H/D	0.5 to 6.0	Hobby: 0.31 to 4.4[122]; Huber and Viskanta, air: 0.25 to 6[123]	Beyond the Hobby range for jets under 0.68 mm at a 3 mm gap
Jet Reynolds number	202 to 2,425 (assumed kinematic viscosity 1.4×10^{-6} m²/s)	Hobby: 70 to 24,000; Rattner: 20 to 500[124125]	Inside the Hobby range; overlaps Rattner for the larger jets

S/D is the pitch of the square grid divided by the jet diameter, and H/D is the impingement gap of 1 to 3 mm divided by the diameter of

0.5 to 2 mm. The kinematic viscosity is an assumed value for 50/50 water-glycol at 65 °C that was not taken from a retrieved source. The correlation ranges are as stated in the cited sources.

The assessment has two parts. The jets in the middle of the diameter range, from about 0.7 to 2 mm, fall inside the spacing ranges of the Hobby correlations, which cover water-like Prandtl numbers. The smallest jets, below about 0.54 to 0.66 mm, require S/D above the Hobby range, and the largest gaps at the smallest diameters require H/D above it. The correlations apply to the geometry of their test articles and extrapolate beyond the stated ranges only with added uncertainty.

6.2 Jets below 0.56 mm exceed the 30 kPa limit at the high flow and low jet count

The design flow of 4 to 8 L/min divided among 100 to 150 jets sets the jet velocity, and the velocity sets the nozzle pressure drop. Table 8 gives the range across the four combinations of jet count and flow for five diameters, using an assumed density of 1,030 kg/m^3 and an assumed kinematic viscosity of 1.4×10^{-6} m^2/s for the coolant. The ideal pressure drop is the velocity head with a discharge coefficient of 1, and the second pressure drop column applies a discharge coefficient of 0.7.[126]

Table 8. Jet velocity, Reynolds number and ideal nozzle pressure drop across the CF-JET flows (derived)

Jet diameter (mm)	Jet velocity (m/s)	Jet Reynolds number	Ideal pressure drop (kPa)	Pressure drop at discharge coefficient 0.7 (kPa)
0.5	2.26 to 6.79	808 to 2,425	2.6 to 23.7	5.4 to 48.5
0.75	1.01 to 3.02	538 to 1,616	0.5 to 4.7	1.1 to 9.6
1.0	0.57 to 1.70	404 to 1,212	0.2 to 1.5	0.3 to 3.0
1.5	0.25 to 0.75	269 to 808	0.03 to 0.29	0.07 to 0.60
2.0	0.14 to 0.42	202 to 606	0.01 to 0.09	0.02 to 0.19

Ranges cover jet counts of 100 and 150 and flows of 4 and 8 L/min. The low end of each range is 150 jets at 4 L/min and the high end is 100 jets at 8 L/min. Values use an assumed density of 1,030 kg/m^3 and an assumed kinematic viscosity of 1.4×10^{-6} m^2/s.

Figure 5. Ideal nozzle pressure drop against jet diameter at the CF-JET flows

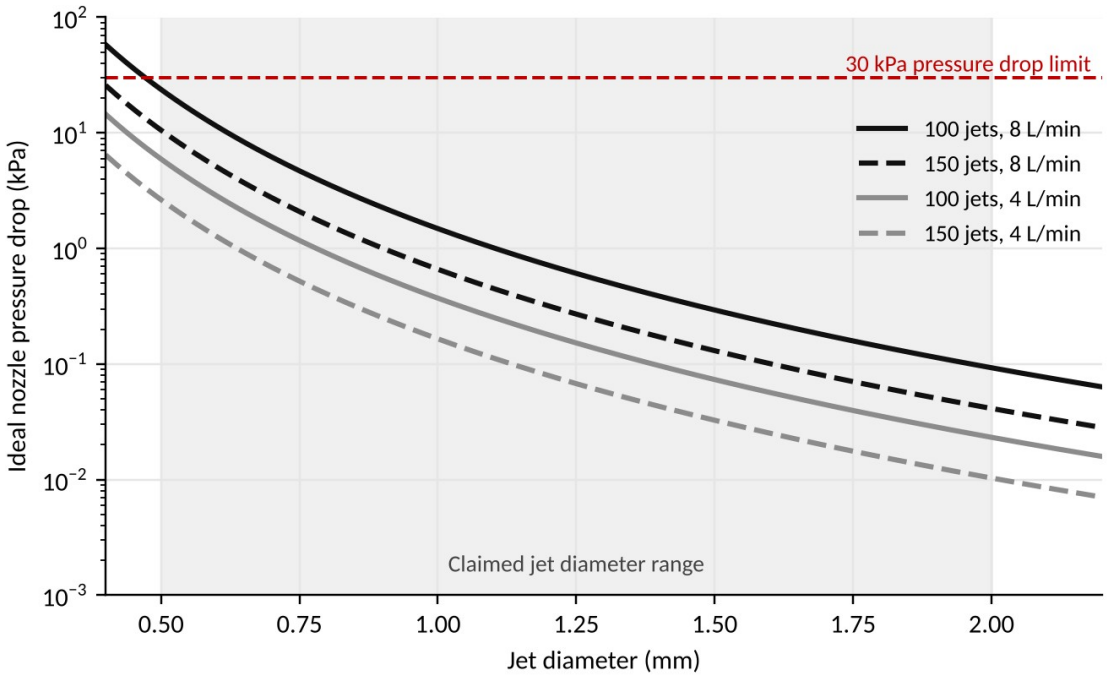

Derived in this paper with an assumed density of 1,030 kg/m³ and a discharge coefficient of 1. The curves are the four combinations of 100 and 150 jets with 4 and 8 L/min, and the shaded band is the claimed diameter range of 0.5 to 2 mm.

For 0.5 mm jets the ideal pressure drop reaches 23.7 kPa at 100 jets and 8 L/min, which is 79 percent of the 30 kPa limit, and 48.5 kPa at a discharge coefficient of 0.7, which is 162 percent of it (derived). The smallest diameter that keeps that case at or below 30 kPa with a discharge coefficient of 0.7 is 0.56 mm, and the smallest that keeps it at or below half the limit is 0.67 mm (derived).[127] At 1 mm and above, the nozzle pressure drop is at most 3.0 kPa, and the jet Reynolds numbers of 202 to 1,212 are in a laminar or transitional range, where the jet coefficient is lower than at the velocities of the 0.5 mm jets. The claimed diameter range therefore spans a nozzle-pressure-limited end and a velocity-limited end, and the combination of diameter, jet count and flow that meets both the 30 kPa limit and the resistance target lies inside it. The sources retrieved do not locate that combination.

Figure 6 combines the nozzle limit with the pitch-to-diameter range of the Hobby correlations over the claimed jet counts.[128] In the claimed range the pitch bound governs, so the window begins near 0.66 mm for 100 jets and 0.54 mm for 150 jets, against nozzle limits of 0.56 mm and 0.46 mm at 8 L/min (derived). A gap of 3 mm adds a bound near 0.68 mm. At 4 L/min the nozzle limit falls to 0.40 mm for 100 jets and 0.33 mm for 150 jets (derived).

Figure 6. Jet diameter and jet count satisfying the nozzle pressure drop limit and the correlation spacing range (derived)

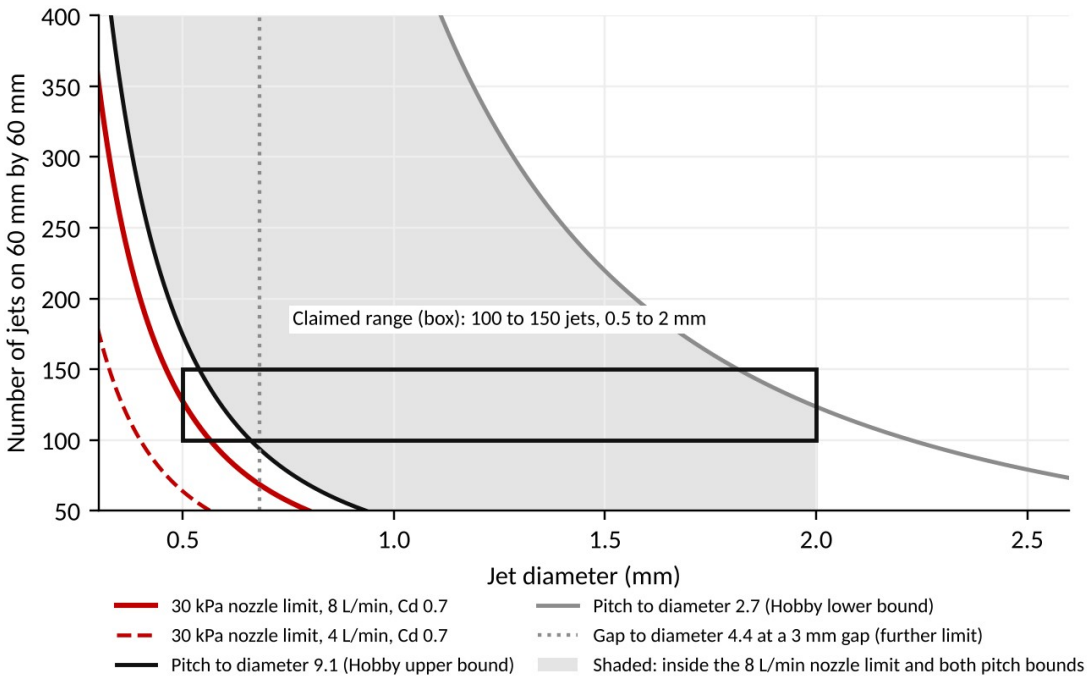

Derived with an assumed density of 1,030 kg/m³ and a discharge coefficient of 0.7. The pitch of the square grid is 60 mm divided by the square root of the jet count. The pitch-to-diameter bounds of 2.7 and 9.1 and the gap-to-diameter bound of 4.4 are the ranges of the Hobby correlations.[129]

6.3 One-piece construction is supported for printed metal bodies and not shown for the full assembly

Kong et al. built a manifold and its microchannels as one aluminum part, and Sun et al. built a jet manifold with optimized channels by laser powder bed fusion.[130][131] Both are cases of printed bodies without brazed joints, and neither has a separate target plate. HRL's printed manifold mates to a skived fin plate, so the block is a two-part design.[132] One-piece construction has conditions in the sources: Kong et al. needed a heat treatment to close pores and reduce leakage, used support pillars and an arch to avoid overhang, and reported a manifold built in an unstable position that became rougher.[133] The CF-JET concept pairs the printed body with a carbon fiber target plate whose coolant face is a thin electroplated metal layer.[134] The sources reviewed do not address the joint or deposited interface between a printed body and a separate target plate, so the claim holds for the printed body and is unproven for the assembly.

Table 9. Assessment of the CF-JET geometry claims against the published record

Claim	Published support	Derived check	Assessment
About 100 to 150 jets	Distributed returns to 40,000 cells on 4 cm² in silicon[135]; nine geometries with extraction ports[136]; no printed metal array at 36 cm² retrieved	Pitch of 4.9 to 6.0 mm on 3600 mm²	Consistent; scale unproven
Jet diameter of 0.5 to 2 mm	Vertical 1 mm channels built to 988 µm; 500 µm channels partly blocked at 22.5° or less[137]; jets under 1 mm reported by a company[138]	Nozzle pressure drop of 2.6 to 23.7 kPa at 0.5 mm; 48.5 kPa at a discharge coefficient of 0.7	Printable with vertical orifice axes; below 0.56 mm exceeds the limit in one case

Claim	Published support	Derived check	Assessment
Grid of 3 to 8 mm	Hobby correlations for S/D of 2.7 to 9.1[139]	S/D of 2.45 to 12.0	Partly outside the correlation range
Impingement gap of 1 to 3 mm	Hobby H/D of 0.31 to 4.4; Huber and Viskanta H/D of 0.25 to 6 in air[140141]; no gap tolerance retrieved	H/D of 0.5 to 6.0	Plausible; gap tolerance unquantified
One-piece construction with no brazed joints	Printed one-piece bodies[142143]; two-part vendor block[144]	Not applicable	Supported for the body; unproven for the assembly

The assessment applies to the sources retrieved for this paper. Derived values use the assumptions stated in the notes to Table 7 and Table 8.

7. Implications for the CF-JET Effort

7.1 Risks

- **Nozzle pressure drop depends on the as-built diameter.** A diameter undersize of 19.5 percent raises the ideal pressure drop by a factor of 2.4, and the 0.5 mm jets already use 79 percent of the 30 kPa limit in the high-flow case (Table 4, Table 8).
- **Scale.** The measured printed coolers have heated areas of 1.0 to 1.44 cm^2, and the CF-JET plate is 25 to 36 times larger. Flow distribution over 100 to 150 orifices has no measured printed precedent in the sources retrieved.
- **Printed imperfections.** A bi-level printed heat sink had pressure drops 8.8 to 30.9 percent above its design and temperature differences of 7.2 to 16.8 percent against simulation.[145]
- **Powder entrapment.** Branching supply and return passages under a 1 to 3 mm gap have no published powder removal procedure, and removal is harder with more bends and smaller diameters.[146]
- **Material properties and leak tightness.** Conductivity of printed AlSi10Mg varied by 18 to 41 percent with annealing, and a printed sink needed heat treatment to close pores.[147148]
- **Dependence on company claims.** The jet-based products with the lowest reported resistances are described in press releases and white papers that omit process data and flow conditions.[149150]

7.2 Design implications

- **Orient the orifices along the build direction.** Vertical channels were the most accurate in the Inconel 718 study, and the jet plate should be built flat with the orifice axes vertical, with supports or arches for its underside.[151152]
- **Size the nozzles from measured data.** Build nozzle coupons in the same build as the plate, measure their diameters by computed tomography and their discharge coefficients on a flow bench, and keep jets above about 0.6 mm until those data exist (Table 8).
- **Add drain and access ports and avoid bends.** Design the return passages with straight paths and ports for powder removal, and inspect the first articles by computed tomography.[153]
- **Test a representative sub-array with and without interleaved returns.** Build both in the same process and test them in the same loop at 4 to 8 L/min and 65 °C, because no published printed jet array provides this baseline (Table 3).

- **Put process limits into the optimization.** Use a minimum wall near 0.3 mm, a fin thickness near 150 µm and a roughness allowance as constraints, and check the optimized geometry by three-dimensional flow models (Table 5, Table 6).[154155156]

7.3 Open research questions

- What discharge coefficient and roughness penalty do printed 0.5 to 2 mm orifices in AlSi10Mg show with water-glycol at 65 °C?
- How is the 30 kPa budget divided among nozzles, plenum and returns for an interleaved printed plate at 4 to 8 L/min?
- What fraction of the single-jet coefficient does the return-port layout retain at 100 to 150 jets on 36 cm²?
- What dimensional tolerance does a 1 to 3 mm gap hold over a span of 60 mm in the printed body?
- Can powder be removed from branching return passages of the CF-JET geometry, and how does the residual powder affect the jets?

8. Conclusion

The published record shows that additive manufacturing can produce one-piece metal manifold coolers with measured resistances of 21 to 94 mm²·K/W on footprints of 1.0 to 1.44 cm², and that manifold and interleaved returns lower pressure drop by 38 to 90 percent against conventional channels in the printed studies. It does not show a printed metal jet array with interleaved returns at the footprint, flow rate and pressure drop of the CF-JET design point.

The claimed geometry is consistent with that record at its center and exceeds it at its edges. Jet counts of 100 to 150 imply a pitch inside the claimed grid, and jets below about 0.56 mm exceed the 30 kPa limit in the high-flow case. Orifice diameter depends on build orientation, and a measured undersize of 19.5 percent raises the ideal nozzle pressure drop by a factor of 2.4. One-piece construction holds for printed bodies and is unproven for an assembly that includes a separate target plate. A program that builds nozzle coupons and a representative sub-array, measures the as-built diameters and gap, and reports the pressure drop partition would close the main gaps in the record.

Bibliography

3DPRINTUK. “Design for Additive Manufacturing, Part 3.” *Assembly Magazine*, 12 December 2022. Trade press. https://www.assemblymag.com/articles/97510-design-for-additive-manufacturing-part-3.

Brunschwiler, Thomas, et al. “Direct Liquid Jet-Impingement Cooling with Micron-Sized Nozzle Array and Distributed Return Architecture.” In *2006 10th IEEE Intersociety Conference on Thermal and Thermomechanical Phenomena in Electronics Systems (ITherm)*, 196–203. 2006.

Butler, C., S. Babu, R. Lundy, R. O’Reilly Meehan, J. Punch, and N. Jeffers. “Effects of Processing Parameters and Heat Treatment on Thermal Conductivity of Additively Manufactured AlSi10Mg by Selective Laser Melting.” *Materials Characterization* 173 (2021): 110945. https://doi.org/10.1016/j.matchar.2021.110945.

Collins, Ivel L., Justin A. Weibel, Liang Pan, and Suresh V. Garimella. “Evaluation of Additively Manufactured Microchannel Heat Sinks.” *IEEE Transactions on Components, Packaging and Manufacturing Technology* (2019). https://doi.org/10.1109/TCPMT.2018.2866972.

CoolIT Systems. “Split-Flow Technology.” Tech brief, n.d. https://coolitsystems.com/wp-content/uploads/2024/05/Split-Flow-Technology-CoolIT-Tech-Brief.pdf.

Gradl, P. R., A. Cervone, and Piero Colonna. “Enhancement of Friction Factors for Microchannels Fabricated Using Laser Powder Directed Energy Deposition.” *Materials & Design* 251 (2025): 113673. https://doi.org/10.1016/j.matdes.2025.113673.

Gupta, Mayank Kumar, Lionel Arnaud, and Kamel Hooman. “2D and 3D Topology Optimization of a Heat-Exchanger Manifold for Flow Distribution in Laminar and Turbulent Regimes.” *Heat Transfer Engineering* (2025). https://doi.org/10.1080/01457632.2025.2578964.

Haber, Ludwig. “JetCool Sub-One System.” Kickoff presentation, ARPA-E COOLERCHIPS program, n.d. https://arpa-e.energy.gov/sites/default/files/2023-11/Day1_03d_JetCoolSubOne_KickOff_Pub.pdf.

Hoang, Cong Hiep, et al. “Design and Thermal Analysis of a 3-D Printed Impingement Pin Fin Cold Plate for Heterogeneous Integration Application.” *IEEE Transactions on Components, Packaging and Manufacturing Technology* (2022). https://doi.org/10.1109/TCPMT.2022.3185401.

Hobby, David, Tom Walker, Alex Rattner, Chris Jacobsen, David Sherrer, and Todd Bandhauer. “Comparison of Experimental and Computational Heat Transfer Characterization of Water Jet Impingement Array with Interspersed Fluid Extraction.” *Heat Transfer Engineering* (2021). https://doi.org/10.1080/01457632.2019.1707404.

Hobby, David Ryan. “Generalized Pressure Drop and Heat Transfer Correlations for Jet Impingement Cooling with Jet Adjacent Fluid Extraction.” PhD diss., Colorado State University, 2022. https://mountainscholar.org/handle/10217/235294.

Huber, Aaron M., and Raymond Viskanta. “Convective Heat Transfer to a Confined Impinging Array of Air Jets with Spent Air Exits.” *Journal of Heat Transfer* 116, no. 3 (1994): 570–576.

Hunter, L. W., D. Brackett, N. Brierley, et al. “Assessment of Trapped Powder Removal and Inspection Strategies for Powder Bed Fusion Techniques.” *International Journal of Advanced Manufacturing Technology* 106 (2020): 4521–4532. https://doi.org/10.1007/s00170-020-04930-w.

International Organization for Standardization and ASTM International. *Additive Manufacturing: Design, Part 1: Laser-Based Powder Bed Fusion of Metals*. ISO/ASTM 52911-1:2019. Geneva: ISO, 2019.

JetCool. “JetCool’s SmartPlate Technology Elevates NVIDIA H100 GPUs with Superior Cooling Efficiency.” Press release, HPCwire, 30 April 2024. https://www.hpcwire.com/off-the-wire/jetcools-smartplate-technology-elevates-nvidia-h100-gpus-with-superior-cooling-efficiency/.

JetCool. “Data Center Liquid Cooling.” Vendor web page, n.d. https://jetcool.com/data-center-liquid-cooling/.

Johnstone, B., C. Saldana, and K. Saleeby. “Slitted Accuracy of Thin Walls in Laser Powder Bed Fusion.” In *Solid Freeform Fabrication 2025: Proceedings of the 36th Annual International Solid Freeform Fabrication Symposium*, 76–88. 2025. https://utw10945.utweb.utexas.edu/sites/default/files/2025/7%20Slit%20Accuracy%20of%20Thin%20Walls%20in%20Laser%20Powder%20Bed%20.pdf.

Kasperovich, G., R. Becker, K. Artzt, P. Barriobero-Vila, G. Requena, and J. Haubrich. “The Effect of Build Direction and Geometric Optimization in Laser Powder Bed Fusion of Inconel 718 Structures with Internal Channels.” *Materials & Design* 207 (2021): 109858. https://doi.org/10.1016/j.matdes.2021.109858.

Kong, Daeyoung, Euibeen Jung, Yunseo Kim, Vivek Vardhan Manepalli, Kyupaeck Jeff Rah, Han Sang Kim, Yongtaek Hong, Hyoung Gil Choi, Damena Agonafer, and Hyoungsoon Lee. “An Additively Manufactured Manifold-Microchannel Heat Sink for High-Heat Flux Cooling.” *International Journal of Mechanical Sciences* 248 (2023): 108228. https://doi.org/10.1016/j.ijmecsci.2023.108228.

Lyons, Sara K. “Characterization of the Effects of Internal Channel Roughness on Fluid Flow and Heat Transfer in Additively Manufactured Microchannel Heat Sinks.” PhD diss., Purdue University, n.d.

https://docs.lib.purdue.edu/dissertations/AAI30506184.

Narumanchi, Sreekant. “Light-Weight, Single-Phase, Liquid-Cooled Cold Plate.” National Renewable Energy Laboratory, U.S. Department of Energy Office of Energy Efficiency and Renewable Energy, 15 May 2012. https://www.energy.gov/eere/vehicles/articles/compact-light-weight-single-phase-liquid-cooled-cold-plate-0.

National Energy Technology Laboratory. “Surface Roughness Effects on Heat Transfer in Additively Manufactured sCO2 Cycle Heat Exchangers.” OSTI record 1819281, n.d. https://www.osti.gov/biblio/1819281.

Ozguc, Serdar, Liang Pan, and Justin A. Weibel. “Topology Optimization of Microchannel Heat Sinks Using a Homogenization Approach.” *International Journal of Heat and Mass Transfer* (2021): 120896. https://doi.org/10.1016/j.ijheatmasstransfer.2020.120896.

Pahinkar, Darshan G., Lauren Boteler, Dimeji Ibitayo, Sreekant Narumanchi, Paul Paret, Douglas DeVoto, Joshua Major, and Samuel Graham. “Liquid Cooled Aluminum Silicon Carbide Heat Sinks for Reliable Power Electronics Packages.” Accepted manuscript, U.S. Department of Energy Public Access, undated. https://www.osti.gov/servlets/purl/1507288.

“Printability and Overall Cooling Performance of Additively Manufactured Holes with Inlet and Exit Rounding.” *Journal of Turbomachinery* 145, no. 3. OSTI record 2418125. https://doi.org/10.1115/1.4056389.

Rattner, Alexander S. “General Characterization of Jet Impingement Array Heat Sinks with Interspersed Fluid Extraction Ports for Uniform High-Flux Cooling.” *Journal of Heat Transfer* 139, no. 8 (August 2017): 082201. https://doi.org/10.1115/1.4036090.

Shepard, Paul. “Microconvective Cooling Produces Very High Heat Transfer Coefficients.” EEPower, 16 July 2019. Trade press. https://eepower.com/news/microconvective-cooling-produces-very-high-heat-transfer-coefficients/.

Smith, David A., Christopher Roper, Jeremy Orosco, and Adam Gross. “Low-Chill™: Hierarchical Manifolds for Data Center Chip Cooling.” White paper, HRL Laboratories, February 2026. https://www.hrl.com/wp-content/uploads/2026/02/HRL-Low-Chill-White-Paper-Feb2026.2.pdf.

SOL Engineering Services, LLC. *CF-JET: AI/ML-Enabled Design and Development of an Additively Manufactured, Liquid-Cooled Jet-Impingement Cold Plate with Optimized Carbon Fiber Target Plate*. Proposal, Rev Final 2, n.d.

Sun, Qidong, Junzhe Guo, Sheng Zhou, Mingji Chen, Da Geng, and Ran Tao. “Synergistic Design of Bi-Level Heat Sink Combining Topology-Optimized Microchannels with Jet Impingement for High-Heat-Flux Applications.” *International Journal of Heat and Mass Transfer* 255 (2026): 127875. https://doi.org/10.1016/j.ijheatmasstransfer.2025.127875.

“Using a Multi-Inlet/Outlet Manifold to Improve Heat Transfer and Flow Distribution of a Pin Fin Heat Sink.” *Journal of Electronic Packaging* 144, no. 3 (September 2022): 031017. https://doi.org/10.1115/1.4054461.

Waye, Scot K., Sreekant Narumanchi, Mark Mihalic, Gilbert Moreno, Kevin Bennion, and Jana Jeffers. “Advanced Liquid Cooling for a Traction Drive Inverter Using Jet Impingement and Microfinned Enhanced Surfaces.” Preprint NREL/CP-5400-61060. Presented at ITherm 2014, Orlando, FL, 27–30 May 2014. National Renewable Energy Laboratory, August 2014. https://www.osti.gov/biblio/1150183.

Wei, Tiwei. “High Efficiency Polymer based Direct Multi-jet Impingement Cooling Solution for High Power Devices.” arXiv:2310.11663. Preprint submitted 18 October 2023. https://arxiv.org/abs/2310.11663.

Wu, Ziheng, Sneha P. Narra, and Anthony Rollett. “Exploring the Fabrication Limits of Thin-Wall Structures in a Laser Powder Bed Fusion Process.” *International Journal of Advanced Manufacturing Technology* 110 (2020): 191–207. https://doi.org/10.1007/s00170-020-05827-4.

Zhou, Yuqing, Tsuyoshi Nomura, and Ercan M. Dede. “Topology Optimization of Manifold Microchannel Heat Sinks.” Conference paper, n.d. Venue not stated in the text read. https://yuqingz.github.io/doc/2020itherm.pdf.

Notes

[1]Daeyoung Kong et al., “An Additively Manufactured Manifold-Microchannel Heat Sink for High-Heat Flux Cooling,” *International Journal of Mechanical Sciences* 248 (2023): 108228, https://doi.org/10.1016/j.ijmecsci.2023.108228.

[2]SOL Engineering Services, LLC, *CF-JET: AI/ML-Enabled Design and Development of an Additively Manufactured, Liquid-Cooled Jet-Impingement Cold Plate with Optimized Carbon Fiber Target Plate*, proposal, Rev Final 2, n.d.

[3]Kong et al., “Additively Manufactured Manifold-Microchannel Heat Sink.”

[4]Ivel L. Collins, Justin A. Weibel, Liang Pan, and Suresh V. Garimella, “Evaluation of Additively Manufactured Microchannel Heat Sinks,” *IEEE Transactions on Components, Packaging and Manufacturing Technology* (2019), https://doi.org/10.1109/TCPMT.2018.2866972.

[5]Cong Hiep Hoang et al., “Design and Thermal Analysis of a 3-D Printed Impingement Pin Fin Cold Plate for Heterogeneous Integration Application,” *IEEE Transactions on Components, Packaging and Manufacturing Technology* (2022), https://doi.org/10.1109/TCPMT.2022.3185401.

[6]David Hobby, Tom Walker, Alex Rattner, Chris Jacobsen, David Sherrer, and Todd Bandhauer, “Comparison of Experimental and Computational Heat Transfer Characterization of Water Jet Impingement Array with Interspersed Fluid Extraction,” *Heat Transfer Engineering* (2021), https://doi.org/10.1080/01457632.2019.1707404.

[7]JetCool, “JetCool’s SmartPlate Technology Elevates NVIDIA H100 GPUs with Superior Cooling Efficiency,” press release, HPCwire, 30 April 2024, https://www.hpcwire.com/off-the-wire/jetcools-smartplate-technology-elevates-nvidia-h100-gpus-with-superior-cooling-efficiency/.

[8]Kong et al., “Additively Manufactured Manifold-Microchannel Heat Sink.”

[9]Collins et al., “Additively Manufactured Microchannel Heat Sinks.”

[10]G. Kasperovich, R. Becker, K. Artzt, P. Barriobero-Vila, G. Requena, and J. Haubrich, “The Effect of Build Direction and Geometric Optimization in Laser Powder Bed Fusion of Inconel 718 Structures with Internal Channels,” *Materials & Design* 207 (2021): 109858, https://doi.org/10.1016/j.matdes.2021.109858.

[11]Qidong Sun et al., “Synergistic Design of Bi-Level Heat Sink Combining Topology-Optimized Microchannels with Jet Impingement for High-Heat-Flux Applications,” *International Journal of Heat and Mass Transfer* 255 (2026): 127875, https://doi.org/10.1016/j.ijheatmasstransfer.2025.127875.

[12]SOL Engineering Services, *CF-JET*, Rev Final 2.

[13]SOL Engineering Services, *CF-JET*, Rev Final 2.

[14]SOL Engineering Services, *CF-JET*, Rev Final 2.

[15]Kong et al., “Additively Manufactured Manifold-Microchannel Heat Sink.”

[16]Kong et al., “Additively Manufactured Manifold-Microchannel Heat Sink.”

[17]Kong et al., “Additively Manufactured Manifold-Microchannel Heat Sink.”

[18]Collins et al., “Additively Manufactured Microchannel Heat Sinks.”

[19]Kong et al., “Additively Manufactured Manifold-Microchannel Heat Sink.”

[20]Collins et al., “Additively Manufactured Microchannel Heat Sinks.”

[21]Hoang et al., “3-D Printed Impingement Pin Fin Cold Plate.”

[22]Sun et al., “Bi-Level Heat Sink.”

[23]Hobby et al., “Water Jet Impingement Array with Interspersed Fluid Extraction.”

[24]Scot K. Waye, Sreekant Narumanchi, Mark Mihalic, Gilbert Moreno, Kevin Bennion, and Jana Jeffers, “Advanced Liquid Cooling for a Traction Drive Inverter Using Jet Impingement and Microfinned Enhanced Surfaces,” preprint NREL/CP-5400-61060, presented at ITherm 2014, Orlando, FL, 27–30 May 2014, National Renewable Energy Laboratory, August 2014, https://www.osti.gov/biblio/1150183.

[25]Hoang et al., “3-D Printed Impingement Pin Fin Cold Plate.”

[26]Hobby et al., “Water Jet Impingement Array with Interspersed Fluid Extraction.”

[27]Tiwei Wei, “High Efficiency Polymer based Direct Multi-jet Impingement Cooling Solution for High Power Devices,” arXiv:2310.11663, preprint submitted 18 October 2023, https://arxiv.org/abs/2310.11663.

[28]Waye et al., “Advanced Liquid Cooling for a Traction Drive Inverter.”

[29]Sreekant Narumanchi, “Light-Weight, Single-Phase, Liquid-Cooled Cold Plate,” National Renewable Energy Laboratory, U.S. Department of Energy Office of Energy Efficiency and Renewable Energy, 15 May 2012, https://www.energy.gov/eere/vehicles/articles/compact-light-weight-single-phase-liquid-cooled-cold-plate-0.

[30]Sun et al., “Bi-Level Heat Sink.”

[31]Collins et al., “Additively Manufactured Microchannel Heat Sinks.”

[32]Serdar Ozguc, Liang Pan, and Justin A. Weibel, “Topology Optimization of Microchannel Heat Sinks Using a Homogenization Approach,”

International Journal of Heat and Mass Transfer (2021): 120896, https://doi.org/10.1016/j.ijheatmasstransfer.2020.120896.

[33]Sara K. Lyons, “Characterization of the Effects of Internal Channel Roughness on Fluid Flow and Heat Transfer in Additively Manufactured Microchannel Heat Sinks,” PhD diss., Purdue University, n.d., https://docs.lib.purdue.edu/dissertations/AAI30506184.

[34]Darshan G. Pahinkar, Lauren Boteler, Dimeji Ibitayo, Sreekant Narumanchi, Paul Paret, Douglas DeVoto, Joshua Major, and Samuel Graham, “Liquid Cooled Aluminum Silicon Carbide Heat Sinks for Reliable Power Electronics Packages,” accepted manuscript, U.S. Department of Energy Public Access, undated, https://www.osti.gov/servlets/purl/1507288.

[35]B. Johnstone, C. Saldana, and K. Saleeby, “Slitted Accuracy of Thin Walls in Laser Powder Bed Fusion,” in *Solid Freeform Fabrication 2025: Proceedings of the 36th Annual International Solid Freeform Fabrication Symposium* (2025), 76–88, https://utw10945.utweb.utexas.edu/sites/default/files/2025/7%20Slit%20Accuracy%20of%20Thin%20Walls%20in%20Laser%20Powder%20Bed%20.pdf.

[36]Waye et al., “Advanced Liquid Cooling for a Traction Drive Inverter.”

[37]Narumanchi, “Light-Weight, Single-Phase, Liquid-Cooled Cold Plate.”

[38]Paul Shepard, “Microconvective Cooling Produces Very High Heat Transfer Coefficients,” EEPower, 16 July 2019, trade press, https://eepower.com/news/microconvective-cooling-produces-very-high-heat-transfer-coefficients/.

[39]JetCool, “SmartPlate Technology Elevates NVIDIA H100 GPUs.”

[40]JetCool, “Data Center Liquid Cooling,” vendor web page, n.d., https://jetcool.com/data-center-liquid-cooling/.

[41]Ludwig Haber, “JetCool Sub-One System,” kickoff presentation, ARPA-E COOLERCHIPS program, n.d., https://arpa-e.energy.gov/sites/default/files/2023-11/Day1_03d_JetCoolSubOne_KickOff_Pub.pdf.

[42]David A. Smith, Christopher Roper, Jeremy Orosco, and Adam Gross, “Low-Chill™: Hierarchical Manifolds for Data Center Chip Cooling,” white paper, HRL Laboratories, February 2026, https://www.hrl.com/wp-content/uploads/2026/02/HRL-Low-Chill-White-Paper-Feb2026.2.pdf.

[43]CoolIT Systems, “Split-Flow Technology,” tech brief, n.d., https://coolitsystems.com/wp-content/uploads/2024/05/Split-Flow-Technology-CoolIT-Tech-Brief.pdf.

[44]JetCool, “SmartPlate Technology Elevates NVIDIA H100 GPUs.”

[45]JetCool, “Data Center Liquid Cooling.”

[46]Shepard, “Microconvective Cooling.”

[47]Haber, “JetCool Sub-One System.”

[48]Smith et al., “Low-Chill™.”

[49]CoolIT Systems, “Split-Flow Technology.”

[50]Kong et al., “Additively Manufactured Manifold-Microchannel Heat Sink.”

[51]Collins et al., “Additively Manufactured Microchannel Heat Sinks.”

[52]Kong et al., “Additively Manufactured Manifold-Microchannel Heat Sink.”

[53]Collins et al., “Additively Manufactured Microchannel Heat Sinks.”

[54]“Using a Multi-Inlet/Outlet Manifold to Improve Heat Transfer and Flow Distribution of a Pin Fin Heat Sink,” *Journal of Electronic Packaging* 144, no. 3 (September 2022): 031017, https://doi.org/10.1115/1.4054461.

[55]Smith et al., “Low-Chill™.”

[56]Aaron M. Huber and Raymond Viskanta, “Convective Heat Transfer to a Confined Impinging Array of Air Jets with Spent Air Exits,” *Journal of Heat Transfer* 116, no. 3 (1994): 570–576.

[57]Huber and Viskanta, “Confined Impinging Array of Air Jets with Spent Air Exits.”

[58]Alexander S. Rattner, “General Characterization of Jet Impingement Array Heat Sinks with Interspersed Fluid Extraction Ports for Uniform High-Flux Cooling,” *Journal of Heat Transfer* 139, no. 8 (August 2017): 082201, https://doi.org/10.1115/1.4036090.

[59]David Ryan Hobby, “Generalized Pressure Drop and Heat Transfer Correlations for Jet Impingement Cooling with Jet Adjacent Fluid Extraction,” PhD diss., Colorado State University, 2022, https://mountainscholar.org/handle/10217/235294.

[60]Thomas Brunschwiler et al., “Direct Liquid Jet-Impingement Cooling with Micron-Sized Nozzle Array and Distributed Return Architecture,” in *2006 10th IEEE Intersociety Conference on Thermal and Thermomechanical Phenomena in Electronics Systems (ITherm)* (2006), 196–203.

[61]Hobby et al., “Water Jet Impingement Array with Interspersed Fluid Extraction.”

[62]Wei, “Direct Multi-jet Impingement Cooling Solution.”

[63]Kong et al., “Additively Manufactured Manifold-Microchannel Heat Sink.”

[64]Kong et al., “Additively Manufactured Manifold-Microchannel Heat Sink.”

[65]Kasperovich et al., “Build Direction and Geometric Optimization.”

[66]Kasperovich et al., “Build Direction and Geometric Optimization.”

[67]Kasperovich et al., “Build Direction and Geometric Optimization.”

[68]Ziheng Wu, Sneha P. Narra, and Anthony Rollett, “Exploring the Fabrication Limits of Thin-Wall Structures in a Laser Powder Bed Fusion Process,” *International Journal of Advanced Manufacturing Technology* 110 (2020): 191–207, https://doi.org/10.1007/s00170-020-05827-4.

[69]Kong et al., “Additively Manufactured Manifold-Microchannel Heat Sink.”

[70]Derived in this paper. For a fixed volumetric flow Q through N orifices of diameter d, the velocity is $v = 4Q/(N\pi d^2)$ and the ideal pressure drop is $\tfrac{1}{2}\rho v^2$, so the pressure drop varies as d^{-4}. The factors in the table use the ratio of the as-built equivalent diameter to the target diameter, with the equivalent diameters measured by Kasperovich et al.

[71]Kasperovich et al., “Build Direction and Geometric Optimization.”

[72]Johnstone, Saldana, and Saleeby, “Slitted Accuracy of Thin Walls.”

[73]Johnstone, Saldana, and Saleeby, “Slitted Accuracy of Thin Walls.”

[74]Ozguc, Pan, and Weibel, “Topology Optimization Using a Homogenization Approach.”

[75]Kong et al., “Additively Manufactured Manifold-Microchannel Heat Sink.”

[76]Collins et al., “Additively Manufactured Microchannel Heat Sinks.”

[77]Kasperovich et al., “Build Direction and Geometric Optimization.”

[78]“Printability and Overall Cooling Performance of Additively Manufactured Holes with Inlet and Exit Rounding,” *Journal of Turbomachinery* 145, no. 3, OSTI record 2418125, https://doi.org/10.1115/1.4056389.

[79]National Energy Technology Laboratory, “Surface Roughness Effects on Heat Transfer in Additively Manufactured sCO2 Cycle Heat Exchangers,” OSTI record 1819281, n.d., https://www.osti.gov/biblio/1819281.

[80]P. R. Gradl, A. Cervone, and Piero Colonna, “Enhancement of Friction Factors for Microchannels Fabricated Using Laser Powder Directed Energy Deposition,” *Materials & Design* 251 (2025): 113673, https://doi.org/10.1016/j.matdes.2025.113673.

[81]Lyons, “Effects of Internal Channel Roughness.”

[82]C. Butler, S. Babu, R. Lundy, R. O’Reilly Meehan, J. Punch, and N. Jeffers, “Effects of Processing Parameters and Heat Treatment on Thermal Conductivity of Additively Manufactured AlSi10Mg by Selective Laser Melting,” *Materials Characterization* 173 (2021): 110945, https://doi.org/10.1016/j.matchar.2021.110945.

[83]Kong et al., “Additively Manufactured Manifold-Microchannel Heat Sink.”

[84]L. W. Hunter, D. Brackett, N. Brierley, et al., “Assessment of Trapped Powder Removal and Inspection Strategies for Powder Bed Fusion Techniques,” *International Journal of Advanced Manufacturing Technology* 106 (2020): 4521–4532, https://doi.org/10.1007/s00170-020-04930-w.

[85]Hunter et al., “Trapped Powder Removal and Inspection Strategies.”

[86]Kong et al., “Additively Manufactured Manifold-Microchannel Heat Sink.”

[87]3DPRINTUK, “Design for Additive Manufacturing, Part 3,” *Assembly Magazine*, 12 December 2022, trade press, https://www.assemblymag.com/articles/97510-design-for-additive-manufacturing-part-3.

[88]Hobby et al., “Water Jet Impingement Array with Interspersed Fluid Extraction.”

[89]Smith et al., “Low-Chill™.”

[90]Wu, Narra, and Rollett, “Fabrication Limits of Thin-Wall Structures.”

[91]Kong et al., “Additively Manufactured Manifold-Microchannel Heat Sink.”

[92]Kasperovich et al., “Build Direction and Geometric Optimization.”

[93]Kasperovich et al., “Build Direction and Geometric Optimization.”

[94]Kasperovich et al., “Build Direction and Geometric Optimization.”

[95]Kong et al., “Additively Manufactured Manifold-Microchannel Heat Sink.”

[96]Collins et al., “Additively Manufactured Microchannel Heat Sinks.”

[97]Kasperovich et al., “Build Direction and Geometric Optimization.”

[98]Johnstone, Saldana, and Saleeby, “Slitted Accuracy of Thin Walls.”

[99]Hunter et al., “Trapped Powder Removal and Inspection Strategies.”

[100]Kong et al., “Additively Manufactured Manifold-Microchannel Heat Sink.”

[101]3DPRINTUK, “Design for Additive Manufacturing, Part 3.”

[102]International Organization for Standardization and ASTM International, *Additive Manufacturing: Design, Part 1: Laser-Based Powder Bed Fusion of Metals*, ISO/ASTM 52911-1:2019 (Geneva: ISO, 2019).

[103]ISO/ASTM, *52911-1:2019*.

[104]Kong et al., “Additively Manufactured Manifold-Microchannel Heat Sink.”

[105]Sun et al., “Bi-Level Heat Sink.”

[106]Yuqing Zhou, Tsuyoshi Nomura, and Ercan M. Dede, “Topology Optimization of Manifold Microchannel Heat Sinks,” conference paper, n.d. (venue not stated in the text read), https://yuqingz.github.io/doc/2020itherm.pdf.

[107]Zhou, Nomura, and Dede, “Topology Optimization of Manifold Microchannel Heat Sinks.”

[108]Ozguc, Pan, and Weibel, “Topology Optimization Using a Homogenization Approach.”

[109]Ozguc, Pan, and Weibel, “Topology Optimization Using a Homogenization Approach.”

[110]Ozguc, Pan, and Weibel, “Topology Optimization Using a Homogenization Approach.”

[111]Wu, Narra, and Rollett, “Fabrication Limits of Thin-Wall Structures.”

[112]Mayank Kumar Gupta, Lionel Arnaud, and Kamel Hooman, “2D and 3D Topology Optimization of a Heat-Exchanger Manifold for Flow Distribution in Laminar and Turbulent Regimes,” *Heat Transfer Engineering* (2025), https://doi.org/10.1080/01457632.2025.2578964.

[113]Sun et al., “Bi-Level Heat Sink.”

[114]Sun et al., “Bi-Level Heat Sink.”

[115]Zhou, Nomura, and Dede, “Topology Optimization of Manifold Microchannel Heat Sinks.”

[116]Ozguc, Pan, and Weibel, “Topology Optimization Using a Homogenization Approach.”

[117]Gupta, Arnaud, and Hooman, “2D and 3D Topology Optimization of a Heat-Exchanger Manifold.”

[118]Sun et al., “Bi-Level Heat Sink.”

[119]Derived in this paper. The pitch is the square root of the footprint area divided by the jet count: √(3600/100) = 6.0 mm and √(3600/150) = 4.9 mm. A pitch of 3 mm gives 400 jets and a pitch of 8 mm gives 56 jets on the same area.

[120]Hobby, “Generalized Pressure Drop and Heat Transfer Correlations.”

[121]Rattner, “General Characterization of Jet Impingement Array Heat Sinks.”

[122]Hobby, “Generalized Pressure Drop and Heat Transfer Correlations.”

[123]Huber and Viskanta, “Confined Impinging Array of Air Jets with Spent Air Exits.”

[124]Hobby, “Generalized Pressure Drop and Heat Transfer Correlations.”

[125]Rattner, “General Characterization of Jet Impingement Array Heat Sinks.”

[126]Derived in this paper. The ideal nozzle pressure drop is $\frac{1}{2}\rho v^2$ with $v = Q/(N \cdot \pi d^2/4)$, and the second column divides it by 0.7^2. The density of 1,030 kg/m³ and the kinematic viscosity of 1.4×10^{-6} m²/s are assumptions for 50/50 water-glycol at 65 °C and were not taken from a retrieved source. The velocity head is the smallest pressure drop at the nozzle. Entrance, plenum and return losses add to it.

[127]Derived in this paper. The pressure drop varies as d^{-4}, so the diameter at which the case of 100 jets and 8 L/min reaches 30 kPa at a discharge coefficient of 0.7 is 0.5 × (48.5/30)^(1/4) = 0.56 mm, and the diameter for 15 kPa is 0.5 × (48.5/15)^(1/4) = 0.67 mm.

[128]Hobby, “Generalized Pressure Drop and Heat Transfer Correlations.”

[129]Hobby, “Generalized Pressure Drop and Heat Transfer Correlations.”

[130]Kong et al., “Additively Manufactured Manifold-Microchannel Heat Sink.”

[131]Sun et al., “Bi-Level Heat Sink.”

[132]Smith et al., “Low-Chill™.”

[133]Kong et al., “Additively Manufactured Manifold-Microchannel Heat Sink.”

[134]SOL Engineering Services, *CF-JET*, Rev Final 2.

[135]Brunschwiler et al., “Direct Liquid Jet-Impingement Cooling.”

[136]Hobby, “Generalized Pressure Drop and Heat Transfer Correlations.”

[137]Kasperovich et al., “Build Direction and Geometric Optimization.”

[138]Shepard, “Microconvective Cooling.”

[139]Hobby, “Generalized Pressure Drop and Heat Transfer Correlations.”

[140]Hobby, “Generalized Pressure Drop and Heat Transfer Correlations.”

[141]Huber and Viskanta, “Confined Impinging Array of Air Jets with Spent Air Exits.”

[142]Kong et al., “Additively Manufactured Manifold-Microchannel Heat Sink.”

[143]Sun et al., “Bi-Level Heat Sink.”

[144]Smith et al., “Low-Chill™.”

[145]Sun et al., “Bi-Level Heat Sink.”

[146]Hunter et al., “Trapped Powder Removal and Inspection Strategies.”

[147]Butler et al., “Thermal Conductivity of Additively Manufactured AlSi10Mg.”

[148]Kong et al., “Additively Manufactured Manifold-Microchannel Heat Sink.”

[149]JetCool, “SmartPlate Technology Elevates NVIDIA H100 GPUs.”

[150]Smith et al., “Low-Chill™.”

[151]Kasperovich et al., “Build Direction and Geometric Optimization.”

[152]Kong et al., “Additively Manufactured Manifold-Microchannel Heat Sink.”

[153]Hunter et al., “Trapped Powder Removal and Inspection Strategies.”

[154]Kong et al., “Additively Manufactured Manifold-Microchannel Heat Sink.”

[155]Ozguc, Pan, and Weibel, “Topology Optimization Using a Homogenization Approach.”

[156]Gupta, Arnaud, and Hooman, “2D and 3D Topology Optimization of a Heat-Exchanger Manifold.”